Supporting Information

Ultrasensitive colorimetric detection of murine norovirus using NanoZyme aptasensor

Pabudi Weerathunge,[a,¶] Rajesh Ramanathan,[a,¶,] Valeria A. Torok,[b] Kate Hodgson,[b] Yun Xu,[c] Royston Goodacre,[c] Bijay Kumar Behera,[d] and Vipul Bansal[a,*]*

[a]Ian Potter NanoBioSensing Facility, NanoBiotechnology Research Laboratory (NBRL), School of Science, RMIT University, GPO Box 2476, Melbourne VIC 3000, Australia.

[b]South Australian Research and Development Institute (SARDI), Food Safety and Innovation, GPO Box 397, Adelaide, SA 5064, Australia.

[c]School of Chemistry, Manchester Institute of Biotechnology, The University of Manchester, 131 Princess Street, Manchester M1 7DN, UK.

[d]ICAR-Central Inland Fisheries Research Institute, Barrackpore, Kolkata 700100, India.

*E-mail: rajesh.ramanathan@rmit.edu.au; Phone: +61 3 9925 2887.

*E-mail: vipul.bansal@rmit.edu.au; Phone: +61 3 9925 2121.

Materials and reagents

Gold (III) chloride ($HAuCl_4.3H_2O$), L-tyrosine, sodium acetate and potassium hydroxide were purchased from Sigma-Aldrich (St. Louis, USA). 3,3,5,5-tetramethylbenzidine (TMB) substrate reagent kit and 30% w/w hydrogen peroxide (H_2O_2) were purchased from BD Sciences and Chem Supply, respectively. The *AG3* aptamer sequence was custom-synthesized and obtained from Integrated DNA Technologies (IDT, USA). Murine norovirus (MNV) and MS2 phage were cultured and quantified at SARDI, Food Safety and Innovation Laboratories, South Australia. The cultures of *Staphylococcus aureus* (ATCC strain 1680) and *Escherichia coli* (ATCC strain K12) were grown on nutrient broth purchased from Amyl Media Pty Ltd. Deionised MilliQ water (18.2 MΩ cm) was used in all the experiments and acquired from Millipore water purification system.

Methods

Briefly, tyrosine-capped GNPs were synthesized as described previously[1-2] and characterized using standard methods. The peroxidase-like NanoZyme activity of GNPs was evaluated by measuring the oxidation of 3,3',5,5'-tetramethylbenzidine (TMB) substrate to a blue coloured product (absorbance signal at *ca*. 650 nm) in the presence of H_2O_2. The enzyme kinetic parameters such as Michaelis-Menten constant, *Vmax*, *Km* and *Kcat* were determined. The most appropriate composition of the GNP-*AG3* aptamer sensor probe was determined through measuring the NanoZyme activity of GNPs after their incubation with different concentrations of the *AG3* aptamers. The ability of the NanoZyme aptasensor to specifically detect MNV was confirmed by exposing different concentrations of a series of bacteria and viruses in the presence and absence of MNV to the sensor probe. The total assay volume was kept constant at 200 µL throughout the study, which contained 20 µL of the GNP NanoZyme sensor probe, 80 µL of the NanoZyme substrate (0.2 mM TMB + 1 mM H_2O_2), and 100 µL

of the analyte sample containing norovirus and/or other contaminants. The regaining of NanoZyme activity due to aptamer desorption from the GNP surface in the presence of norovirus was measured and was used for calculating the sensor response. Sensor response is represented as A/A_0 where A is the absorbance obtained after 10 min of incubation after the addition of TMB and H_2O_2 while A_0 represents the value obtained before the addition of TMB and H_2O_2. Important sensor parameters such as linear dynamic operating range, LoD, accuracy and precision were calculated using well-established algorithms. The real-world applicability of the sensor was evaluated by determining the sensor response towards norovirus in the presence of other contaminants including extremely high relative concentrations of the MS2 phage, *E. coli*, *S. aureus*, human serum and shellfish homogenate. For determination of norovirus in human serum, MNV of appropriate concentration were directly prepared in undiluted serum. For determination of MNV in shellfish, two mussels obtained from local supermarket were ground with 50 mL of deionised water; the shellfish homogenate was spiked with a pre-determined MNV concentration and filtered using a 0.45 μm syringe filter prior to use.

Synthesis of tyrosine-functionalized gold nanoparticles (GNPs). Tyrosine-functionalized GNPs were synthesized according to the previously reported procedure.[1, 3-4] **Fig. S1** shows a schematic representing the reduction process involved during the formation of GNPs. In brief, 100 mL of L-tyrosine and potassium hydroxide (0.1 mM) were added to a flat bottom flask. Under vigorous stirring and boiling conditions, 0.2 mM equivalent of $HAuCl_4$ was injected and the solution was stirred under boiling for an additional five minutes. The solution changed colour from pale yellow to ruby red, suggesting the formation of GNPs. The potentially unreacted tyrosine and gold ions were removed by dialysis (24 h) using 12 kDa molecular cut-off cellulose dialysis membrane. The concentration of the dialyzed GNPs was determined by atomic absorption spectroscopy using a Varian Fast Sequential AAS after

digesting the GNPs in concentrated nitric acid. During the reduction of $AuCl_4^-$ there is a concomitant oxidation of the amino acid tyrosine, which binds to the surface of the GNP through the amine group leading to its stabilization, as established in our previous work.[1]

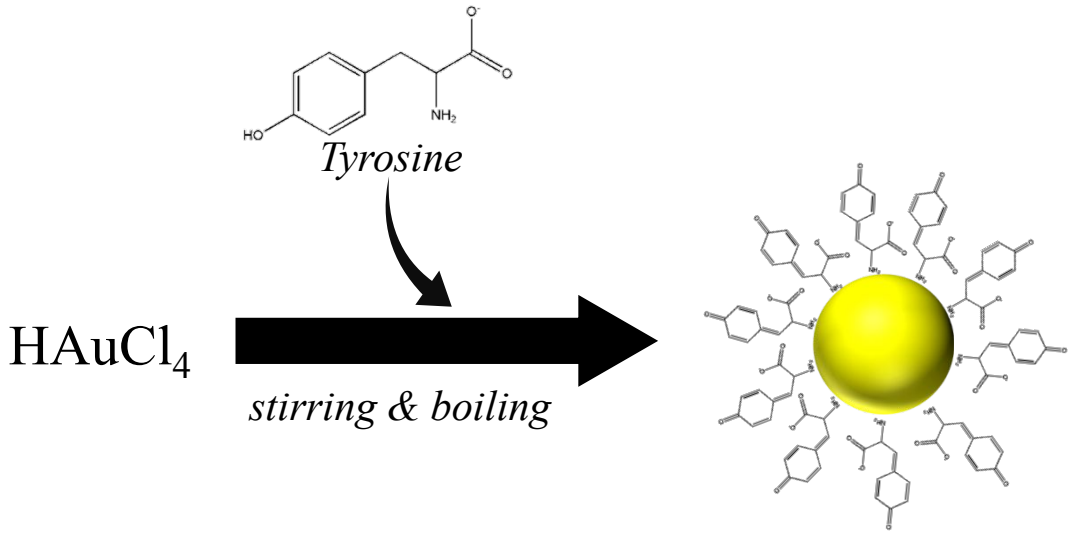

Fig. S1. *Schematic representation of the synthesis of tyrosine-functionalized gold nanoparticles (**GNPs**).*

Characterization of tyrosine-functionalized GNPs. Following the synthesis and dialysis of tyrosine-functionalized GNPs, the nanoparticles were first characterized using UV-visible absorbance spectroscopy. The absorbance spectrum was obtained on a Cary 50 Bio-spectrophotometer with a 1 cm path length. **Fig. S2**a shows the UV-vis absorbance spectrum obtained from the GNPs. A typical surface plasmon resonance (SPR) feature at *ca*. 520 nm was observed. This is a characteristic feature of GNPs and is consistent with previous reports.[1, 5-7] The absence of additional bands in the near infrared region suggests that the GNPs are quasi-spherical in shape while the sharpness of the SPR feature suggesting a narrow particle size distribution.

The morphology of the GNPs was confirmed using transmission electron microscopy (TEM). The sample for TEM was prepared by drop coating a solution containing the GNPs on to a

carbon coated copper grid and analysed on a JEOL 1010 TEM instrument operated at an accelerating voltage of 100 kV. TEM analysis confirmed the quasi-spherical morphology with an average diameter of 20-25 nm (inset in Fig. S2a), which is consistent with previous reports.[3-4] The crystalline nature of the GNPs was also assessed by X-ray diffraction (XRD) obtained on a Bruker AXS X-ray diffraction system operated at a voltage of 40 kV and current of 40 mA with Cu Kα radiation. Well-defined Bragg reflections corresponding to (111), (200), (220), (311) and (222) planes, which could be indexed based on the face centered cubic (fcc) lattice structure of crystalline Au were observed (**Fig. 2**b).[8]

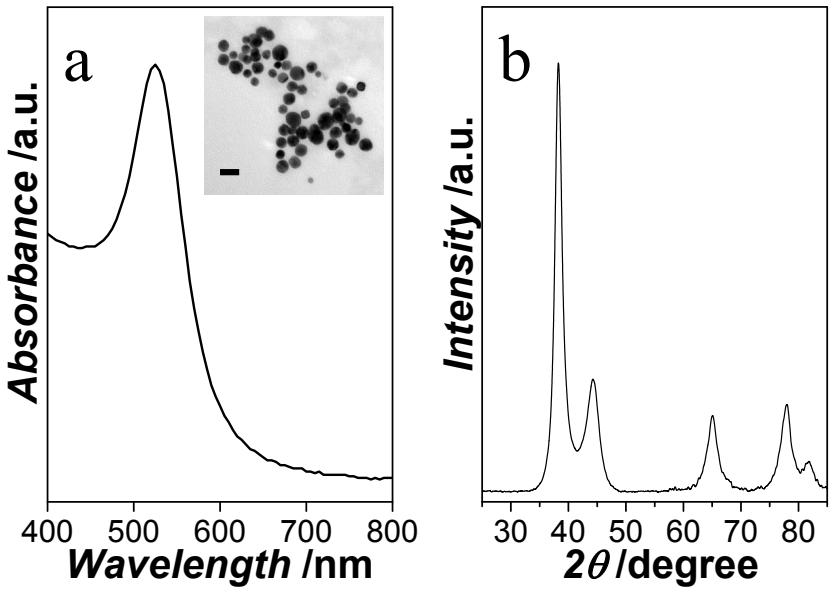

Fig. S2. *(a) UV-visible absorbance spectrum obtained from pristine GNPs, while the inset shows the representative TEM image (scale bar: 50 nm). (b) XRD pattern obtained from tyrosine-functionalized GNPs showing typical Bragg reflections corresponding to fcc gold.*

Evaluation of the enzyme-like (NanoZyme) characteristics of tyrosine-functionalized GNPs. The NanoZyme activity of GNPs was evaluated by assessing their catalytic ability to oxidize 3,3',5,5'-tetramethylbenzidine (TMB) substrate to a blue coloured product in the presence of H_2O_2. The oxidation of TMB leads to a relatively stable colour product (blue colour measured using a Perkin Elmer multimode plate reader), characterised by a typical

absorbance signal at *ca*. 650 nm.[9] The peroxidase-like NanoZyme activity of GNPs increased as a function of GNP concentration (**Fig. S3**a). Similar to that typically observed in other nanomaterials, the NanoZyme activity also showed dependence on the TMB (Fig. S3b) and H_2O_2 concentration (Fig. S3c).

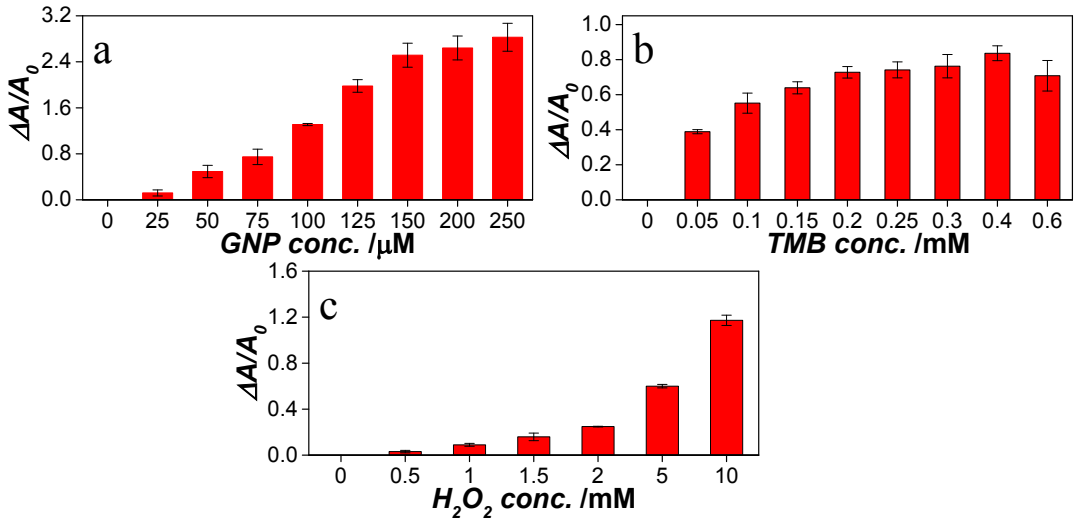

Fig. S3. *Influence of (a) GNP concentration, (b) TMB concentration and (c) H_2O_2 concentration on the peroxidase-like NanoZyme activity of tyrosine-functionalized GNPs. The plots show the mean of 5 measurements and the error bars show standard deviation.*

Determination of kinetic parameters of NanoZyme-driven colorimetric reaction. The enzyme kinetic parameters such as Michaelis-Menten constant (*Km*), maximum initial velocity (*Vmax*) and turnover number (*Kcat*) were determined to assess the catalytic performance of GNPs. The NanoZyme activity increased as a function of increasing TMB and H_2O_2 concentration where a non-linear curve fit of the reaction velocity showed characteristic Michaelis-Menten curves (**Fig. S4**). All fittings were performed using OriginPro 2016 with Michaelis-Menten enzyme kinetic model and Levenberg Marquardt iteration algorithm.

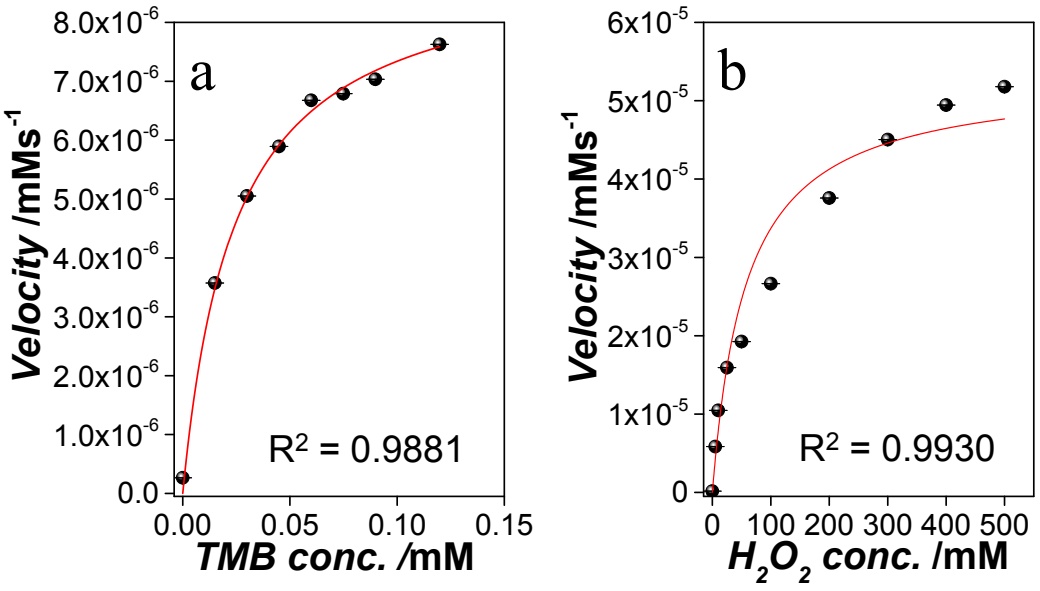

Fig. S4. *The Michaelis-Menten constant (Km) and maximum reaction velocity (Vmax) shown by tyrosine-functionalized GNPs. The steady state kinetics observed in the GNPs with different (a) TMB and (b) H_2O_2 concentrations. The plots show the mean of 5 measurements and the error bars show standard deviation.*

The Michaelis-Menten constant and reaction velocity are listed in **Table S1**. *Km* represents the affinity of the nanoparticle to the substrate (lower *Km* value = higher affinity). The catalytic constant (efficiency) K_{cat} also known as the turnover number was calculated using the following equation:

$$K_{cat} = \frac{V_{max}}{[E]}$$

where [E] represents the nanoparticle concentration. The obtained values for enzyme kinetic parameters were comparable to the values reported in the literature for GNPs as well as other nanoparticles.[10-11]

***Table S1**: Enzyme kinetic parameters obtained for tyrosine-functionalized GNPs at pH 4.*

Substrate	*Km* [mM]	*Vmax* [mM/s]	*Kcat* [/s]
TMB	0.024	9.13×10^{-6}	9.13×10^{-5}
H_2O_2	57.84	5.32×10^{-5}	5.32×10^{-4}

Sensor probe fabrication, determination of binding parameters and sensor probe stability. The molecular recognition element (MRE) in the sensor provides target specificity, which is an important aspect in biosensor development. Aptamers have recently emerged as excellent MREs and suggested to be a viable alternative to antibodies used in conventional ELISA.[12-14] In the current study, we used the *AG3* aptamer (5′GCTAGCGAATTCCGTACGAAGGGCGAATTCCACATTGGGCTGCAGCCCGGGG GATCC3′) that was previously raised specifically against MNV[15] using systematic evolution of ligands by exponential enrichment (SELEX). This aptamer was raised against the surface of the virus capsid and is therefore able to directly detect the virus without the need for viral RNA extraction. Given the high specificity of aptamers in recognizing its target, we envisage that the use of *AG3* aptamer as an MRE would provide outstanding specificity to our NanoZyme aptasensor.

For the fabrication of the sensor probe, the aptamers were first heated at 92 °C for 10 min, followed by snap-chilling on ice for 5 min to allow the temperature to fall to room temperature. The high structural flexibility of aptamers allows them to uncoil exposing its nitrogenous bases. The high affinity of nitrogenous bases to GNPs allows for a coordination interaction between the nitrogenous bases and GNPs leading to a non-covalent adsorption of the aptamer on the surface of GNP.[16] Different concentrations (0 – 200 nM) of aptamer solution were incubated with 75 μM concentration of GNPs for 5 min at 37 °C. The

NanoZyme activity of the GNP-aptamer nanoconjugate was evaluated by adding TMB/H_2O_2 and monitoring the change in colour using UV-visible spectroscopy in a multimode plate reader. The decrease in the NanoZyme activity as a function of aptamer concentration was fitted using reverse Hill equation and the obtained association constant (K_a) and Hill coefficient (n) are presented in **Table S2**.

Table S2: *Binding parameters obtained for sensor probe from reverse Hill fitting.*

GNP conc. [μM]	K_a [M^{-1}]	Hill coefficient [n]	R^2
75	$(4.5\pm2.6) \times 10^7$	1.91	0.9984

We also estimated the number of aptamers required to block the NanoZyme activity of a single GNP in the sensor probe. To achieve this, we first needed to establish the number of GNPs present in the reaction. This was achieved by first calculating the mass of each GNP of 20 nm diameter, based on which the total number of GNPs in the reaction could be estimated. Briefly, considering that the average diameter of the GNPs used in our study is 20 nm, the volume of one GNP corresponds to 4.191×10^{-18} cm^3. Given that the density of Au is 19.32 g/cm^3, the mass of a GNP of 20 nm diameter is 8.096×10^{-17} g. The number of moles of Au available in the reaction is 1.5×10^{-8} moles, which corresponds to 2.95×10^{-6} g of Au (molecular weight of Au is 196.96657). Therefore, the number of GNPs present in the total reaction will correspond to 3.65×10^{10} particles. Similarly, the number of aptamers present in the reaction can also be calculated based on the moles of aptamers in the reaction. With 75 nM concentration of aptamers in 200 μL volume, the total moles of aptamers available to interact with GNPs correspond to 1.5×10^{-11} moles, which is equivalent to 9.035×10^{12} aptamer molecules in the reaction. Therefore, the NanoZyme activity of each GNP is estimated to be blocked in the sensor probe by an average of ~250 aptamers molecules.

Next, the colloidal stability of the GNP-aptamer nanoconjugate (sensor probe) was assessed using UV-visible spectroscopy and TEM analysis. The UV-visible spectra (**Fig. S5**) obtained from the GNP-aptamer conjugate shows no change in the SPR feature to that obtained in the case of pristine GNPs (shown previously in Fig. S2). This suggests that surface passivation of the GNP with aptamers did not lead to aggregation. TEM analysis further confirms that there was no change in the size and morphology of the GNPs confirming the stability of the sensor probe.

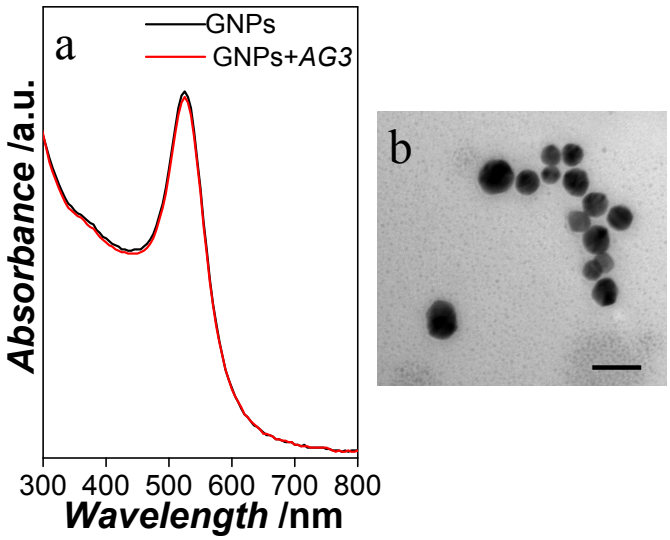

Fig. S5. *(a) UV-visible spectra and the (b) TEM image of AG3-conjugated GNP obtained at the highest aptamer concentration (200 nM). Scale bar in TEM corresponds to 50 nm.*

Preparation of murine norovirus (MNV) culture. MNV-1 (ATCC® PTA-5935™) was propagated in RAW 264.7 (ATCC® TIB-71) cells, which were maintained according to ATCC recommendations. In brief, flasks of confluent RAW 264.7 cells were infected with 5 mL/flask of a MNV suspension with a multiplicity of infection of 1 and incubated for 60 min at 37 °C with gentle rocking. DMEM-10 was added to each flask and incubated for 24-48 h at 37 °C and 5% CO_2 until cell lysis was evident. The medium was collected and centrifuged at 1,500 rpm for 5 min at 4°C to remove cellular debris. The viable virus titer was determined

by plaque assay.[17] RAW 264.7 cells were seeded into 6-well plates at a density of 1×10^6 viable cells/mL in DMEM-10 and incubated overnight at 37 °C and 5% CO_2. Viral supernatant was serially diluted ten-fold in DMEM-5. Medium was removed from the RAW 264.7 cells and 0.5 mL of the viral dilution series was added to wells in duplicate and incubated for 1 h at ambient temperature. Following incubation, the virus inoculum was removed and 2 mL of molten agarose overlay preparation was added to each well and incubated for 48-72 h at 37 °C and 5% CO_2. Neutral red staining solution was added to each well and incubated for 1-3 h at room temperature and the virus titer calculated in plaque forming units (pfu) per mL.

Preparation of MS2 phage viral culture. MS2 phage (NCTC 12487) were propagated in *Salmonella enterica* subsp. *enterica*, WG49 (NCTC 12484).[18] WG49 was inoculated into 50 mL tryptone yeast extract glucose broth (TYGB) containing 1% calcium/glucose solution and incubated at 37 °C for 18 h. The overnight culture (500 µL) was sub-cultured into 50 mL fresh TYGB containing 1% calcium/glucose solution and incubated at 37 °C for 90 min. This culture was inoculated with 500 µL of MS2 phage stock and incubated at 37 °C for 5 h. Chloroform (1:10 ratio) was added, followed by storage at 4 °C for 18 h. The phage suspension was aspirated and centrifuged at 3,000 × g for 20 min to remove cellular debris. The MS2 phage stock was adjusted to a concentration of 10^7 pfu/mL and 5% v/v glycerol was added before storage at -80 °C. The MS2 phage titre was determined by plaque assay.[18] In brief, the host bacteria, *Salmonella* WG49 was cultured to early log phase in TYGB containing 1%v calcium/glucose solution. The MS2 phage stock was serially diluted to 10^{-10} in 0.1% peptone water. Following incubation of the *Salmonella* WG49, 1mL of host culture was added to 2.5 mL tryptone yeast extract glucose agar 1% (TYGA1) overlay supplemented with 1% calcium/glucose solution, along with 1 mL of the MS2 phage dilutions in duplicate. The overlays were poured onto tryptone yeast extract glucose agar 2% (TYGA2) plates

supplemented with 1% calcium/glucose solution and incubated for 18 h at 37 °C. The plaques were counted and the titre expressed as pfu/mL.

Preparation of bacterial cultures. ATCC strain of *Staphylococcus aureus* 1680 and *Escherichia coli* K12 were procured, maintained and cultured in nutrient broth (NB). The bacteria were grown and the optical density at 600 nm was maintained at 1.0. The cells were collected by centrifugation (performed at 4 °C) at 3,000 × g for 10 min and the pellets were washed three times with 10 × phosphate buffer saline (PBS). The bacteria thus obtained were dispersed in 1 × PBS and quantified using a haemocytometer before using them for sensing experiments.

Sensor operation and evaluation of sensor parameters. The ability of the NanoZyme aptasensor to specifically detect norovirus was evaluated by exposing a predetermined number of MNV (based on plaque assay) to the sensor probe in a 96 well plate format for 10 min. The total assay volume was kept constant at 200 µL, which contained 20 µL of the GNP NanoZyme sensor probe, 80 µL of the NanoZyme substrate (0.2 mM TMB + 1 mM H_2O_2), and 100 µL of the analyte sample containing norovirus and/or other contaminants. The regaining of NanoZyme activity due to aptamer desorption from the surface of GNP sensor probes in the presence of norovirus was measured using an ELISA plate-reader at $A_{650\ nm}$.

The dynamic linear range of the detection was obtained by plotting the sensor response with increasing MNV concentration, while the line of best fit was calculated using Origin Pro software using direct weighting. The limit of detection (LoD) was estimated from the equation $3(STD_{blank}/m)$, where STD_{blank} is the standard deviation of the colorimetric signal of the blank and m is the slope of the linear fit.

The reaction velocity of the sensor response in the presence and absence of different number of MNVs at the sensing time-point was calculated using enzyme kinetic theory. Considering

that the assay was performed at pH 7, the V_{max} was first recalculated and was determined to be 3.99×10^{-6} mMs^{-1}. The reaction velocity for the sensor probe as well as the response obtained at different MNV concentrations was then calculated using *Beer-Lambert* law and is presented in the main manuscript (Fig. 2). The relative increase in the reaction velocity was plotted as a function of MNV concentration (**Fig. S6**), where a linear relationship is obtained. This is unsurprising as the reaction velocity is calculated from the sensor response. The regression analysis from the linear fit further suggests that the reaction velocity would improve 37% at the calculated LoD of 3 norovirus.

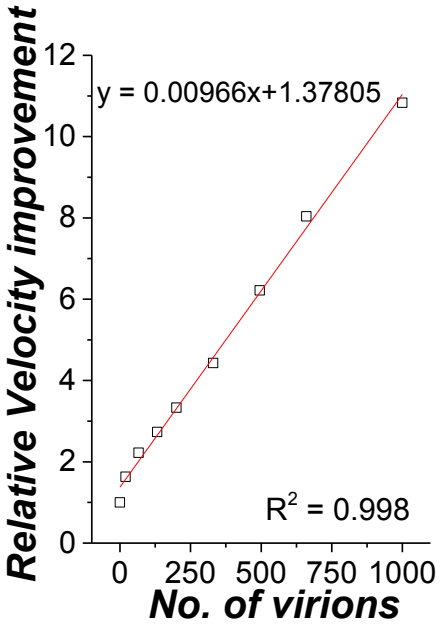

Fig. S6. *Linear regression analysis of the improvement in the reaction velocity calculated using Beer-Lambert's law, when sensor probe is exposed to different numbers of MNVs.*

Important sensor parameters such as the accuracy and the precision of the biosensor were calculated for the sensor response obtained using 75 µM GNP concentration by considering the results obtained from 20 independent events. The accuracy was determined by using (*n*/*N*)*100 formula at a significance level of 0.05 and 0.1 where *n* represent the sensing events that fall within the target MNV numbers (as determined by plaque forming units

representing infective viral load) and *N* is the total number of test events. The % precision was calculated by the coefficient of variation (CoV) method using the formula %Precision = 100 - %CoV. Furthermore, the accuracy and precision of sensor response was determined by performing three independent set of experiments, such that the response was tested using sensor probes prepared in a single batch (in-batch), intra-batch *i.e*. creating the sensor probe on different days using GNPs prepared in a single batch and inter-batch variations *i.e.* creating the sensor probe using two independently synthesized GNPs. This allowed us to determine the robustness of the sensor response against three independent MNV concentrations (Table S3).

Table S3. *In-batch, intra-batch and inter-batch variation in the precision and accuracy of the NanoZyme aptasensor during MNV detection.*

Batch	Target number of MNV	Accuracy [%] (at 0.05 / 0.1 significance level)	Precision [%]
In-batch	20	95 / 100	97.3
	200	100 / 100	98.9
	1000	100 / 100	99.3
Intra-batch	20	95 / 100	96.9
	200	100 / 100	99.2
	1000	100 / 100	98.1
Inter-batch	20	95 / 100	95.9
	200	100 / 100	97.6
	1000	100 / 100	98.9

Controlling the dynamic range of sensor operation. When the sensor probe was fabricated using 75 μM GNP concentration, the sensor saturates beyond 1000 MNVs, *i.e*. the sensor response does not follow the linear dynamic range beyond this virus number. We overcome this issue by changing the GNP concentration from 75 μM to 100 μM and 150 μM during

fabrication of sensor probes. With the increasing GNP concentration during sensor probe fabrication, the number of aptamers required to passivate the GNP surface also increased. This meant that the linear operating range of the sensor could be shifted towards higher dynamic ranges. This allowed us to actively modulate the linear dynamic range of operation from 20-1,000 MNV per assay obtained at 75 µM GNP concentration to 132-1,980 at 100 µM and 330-3,300 MNV per assay at 150 µM GNP concentration. The estimated LoD for these respective cases corresponded to 3, 5 and 8 MNV per assay (Fig. S7). Considering that our NanoZyme assays utilised 100 µL of original norovirus samples, the effective LoD equates to the norovirus concentration of 30, 50 and 80 viruses/mL in the original analyte sample.

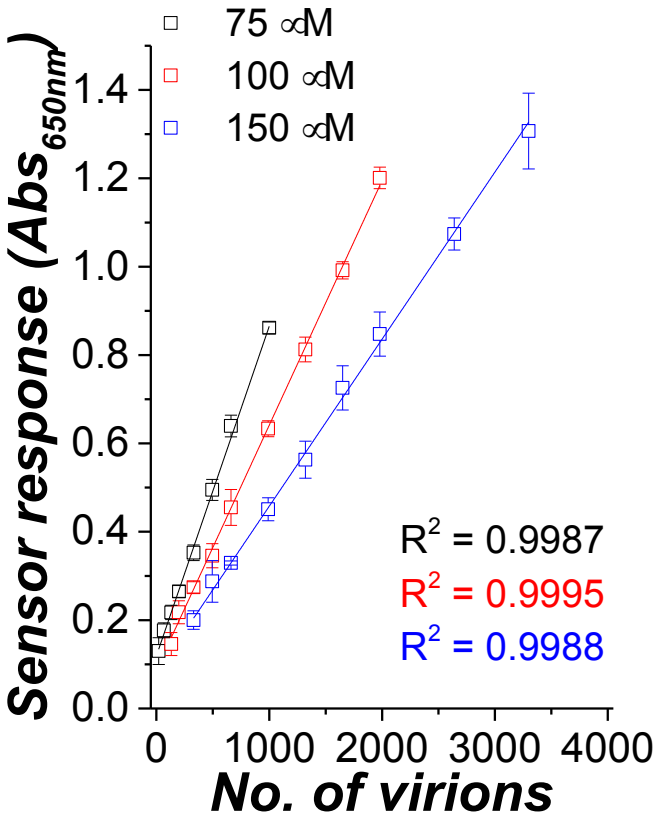

Fig. S7. *NanoZyme aptasensor response in the presence of increasing concentration of MNV, while using sensor probes fabricated using three independent GNP concentrations, as*

indicated in the graph. The corresponding lines show the linear fits of the sensor response. The plots show the mean of 5 measurements and the error bars show standard deviation.

Comparison of the current NanoZyme aptasensor with other previously reported norovirus biosensors for determining effective detection limit (LoD). A recent study showed the ability of antibody-conjugated hybrid materials for the detection of NoV virus like particles (VLP), a non-infective surrogate of norovirus[19] The study showed the ability to detect NoV VLP at concentrations with limit of detection (LoD) as low as 10^2 pg/mL, which was significantly better than a commercial kit (>10^3 pg/mL) and conventional ELISA (>10^4 pg/mL). To enable comparison of our sensor performance to prior studies, we converted reported protein concentrations to the equivalent of VLP or norovirus,[20] a unit more representative of a potentially infective virus particle. Based on the volume of original samples employed in different studies (Table 1, main manuscript), we also converted the detection limits to the concentration of norovirus/mL in the original analyte sample, as this allows the true assessment of the potential of the reported sensor technology for real-world sensing. Furthermore, it is noted that in our current study, the focus has been on determining the amount of infective norovirus present in the sample, as we were able to determine the original infective MNV concentration by plaque forming assays instead of focussing on overall protein concentration of virus that may include both infective and non-infective viruses. In regards to calculations, given that each virus particle is composed of 180 capsid proteins with a predicted molecular weight (MW) of 58,000 Da per capsid protein, each virus capsid particle would therefore have a molecular weight of 10,440,000 Da. VLP/mL can then be calculated using the formula VLP/mL = (protein concentration in mg/mL x 10^{-9} x Avogadro's constant)/MW in Da. These calculations have been used for comparison of different norovirus sensors reported in Table 1.

Cross reactivity studies to determine the specificity of the NanoZyme aptasensor. The sensor response in terms of the colorimetric response at 650 nm in the presence and absence of murine norovirus is shown in **Table S4**, where the respective controls in various matrices in the absence of MNVs is also shown.

Table S4. *Colorimetric response of the sensor detected under various matrices.*

Sample	20	200	1000
Probe	0.05 ± 0.00564	0.05 ± 0.00564	0.05 ± 0.00564
NoV	0.1298 ± 0.0301	0.26502 ± 0.01333	0.86168 ± 0.01318
MS2 phage	0.0623 ± 0.0044	0.06975 ± 0.00935	0.08341 ± 0.00546
MS2 phage + NoV	0.1256 ± 0.03512	0.27646 ± 0.01441	0.87298 ± 0.01333
S. aureus	0.0689 ± 0.00938	0.07238 ± 0.00349	0.07998 ± 0.0053
S. aureus + NoV	0.12968 ± 0.0224	0.28012 ± 0.02066	0.89276 ± 0.01756
E. coli	0.07458 ± 0.0034	0.07876 ± 0.00489	0.08763 ± 0.00941
E. coli + NoV	0.12723 ± 0.01683	0.25978 ± 0.02246	0.87672 ± 0.0245
Serum	0.08348 ± 0.00535	0.08824 ± 0.00784	0.09378 ± 0.00437
Serum + NoV	0.1487 ± 0.01641	0.2813 ± 0.01293	0.89998 ± 0.01318
Shellfish	0.08349 ± 0.0089	0.08929 ± 0.00507	0.09356 ± 0.00783
Shellfish + NoV	0.128 ± 0.0492	0.23249 ± 0.05104	0.80529 ± 0.05321

Supporting References.

1. Selvakannan, P.; Ramanathan, R.; Plowman, B. J.; Sabri, Y. M.; Daima, H. K.; O'Mullane, A. P.; Bansal, V.; Bhargava, S. K., Probing the effect of charge transfer enhancement in off resonance mode SERS via conjugation of the probe dye between silver nanoparticles and metal substrates. *Phys. Chem. Chem. Phys.* **2013,** *15*, 12920-12929.
2. Daima, H. K.; Selvakannan, P. R.; Shukla, R.; Bhargava, S. K.; Bansal, V., Fine-Tuning the Antimicrobial Profile of Biocompatible Gold Nanoparticles by Sequential Surface Functionalization Using Polyoxometalates and Lysine. *PLOS ONE* **2013,** *8*, e79676.
3. Weerathunge, P.; Ramanathan, R.; Shukla, R.; Sharma, T. K.; Bansal, V., Aptamer-controlled reversible inhibition of gold nanozyme activity for pesticide sensing. *Anal. Chem.* **2014,** *86*, 11937-11941.
4. Sharma, T. K.; Ramanathan, R.; Weerathunge, P.; Mohammadtaheri, M.; Daima, H. K.; Shukla, R.; Bansal, V., Aptamer-mediated 'turn-off/turn-on' nanozyme activity of gold nanoparticles for kanamycin detection. *Chem. Commun.* **2014,** *50*, 15856-15859.

5. Vilela, D.; González, M. C.; Escarpa, A., Sensing colorimetric approaches based on gold and silver nanoparticles aggregation: chemical creativity behind the assay. A review. *Anal. Chim. Acta* **2012,** *751*, 24-43.
6. Liu, X.; Wang, Q.; Zhao, H.; Zhang, L.; Su, Y.; Lv, Y., BSA-templated MnO2 nanoparticles as both peroxidase and oxidase mimics. *Analyst* **2012,** *137*, 4552-4558.
7. Saha, K.; Agasti, S. S.; Kim, C.; Li, X.; Rotello, V. M., Gold nanoparticles in chemical and biological sensing. *Chem. Rev.* **2012,** *112*, 2739-2779.
8. Reddy, A. S.; Chen, C.-Y.; Chen, C.-C.; Jean, J.-S.; Chen, H.-R.; Tseng, M.-J.; Fan, C.-W.; Wang, J.-C., Biological synthesis of gold and silver nanoparticles mediated by the bacteria Bacillus subtilis. *J. Nanosci. Nanotechnol.* **2010,** *10*, 6567-6574.
9. Josephy, P. D.; Eling, T.; Mason, R. P., The horseradish peroxidase-catalyzed oxidation of 3, 5, 3', 5'-tetramethylbenzidine. Free radical and charge-transfer complex intermediates. *J. Biol. Chem.* **1982,** *257*, 3669-3675.
10. Jv, Y.; Li, B.; Cao, R., Positively-charged gold nanoparticles as peroxidiase mimic and their application in hydrogen peroxide and glucose detection. *Chem. Commun.* **2010,** *46*, 8017-8019.
11. Wang, S.; Chen, W.; Liu, A. L.; Hong, L.; Deng, H. H.; Lin, X. H., Comparison of the peroxidase-like activity of unmodified, amino-modified, and citrate-capped gold nanoparticles. *ChemPhysChem* **2012,** *13*, 1199-1204.
12. Asati, A.; Santra, S.; Kaittanis, C.; Nath, S.; Perez, J. M., Oxidase-like activity of polymer-coated cerium oxide nanoparticles. *Angew. Chem. Int. Edition.* **2009,** *48*, 2308-2312.
13. Keefe, A. D.; Pai, S.; Ellington, A., Aptamers as therapeutics. *Nat. Rev. Drug Discov.* **2010,** *9*, 537-550.
14. Song, K.-M.; Lee, S.; Ban, C., Aptamers and their biological applications. *Sensors* **2012,** *12*, 612-631.
15. Giamberardino, A.; Labib, M.; Hassan, E. M.; Tetro, J. A.; Springthorpe, S.; Sattar, S. A.; Berezovski, M. V.; DeRosa, M. C., Ultrasensitive norovirus detection using DNA aptasensor technology. *PLoS One.* **2013**, e79087.
16. Li, H.; Rothberg, L., Colorimetric detection of DNA sequences based on electrostatic interactions with unmodified gold nanoparticles. *Proc. Natl. Acad. Sci. USA* **2004,** *101*, 14036-14039.
17. Gonzalez-Hernandez, M. B.; Cunha, J. B.; Wobus, C. E., Plaque assay for murine norovirus. *J. Vis. Exp.* **2012**, e4297.
18. Hodgson, K. R.; Torok, V. A.; Turnbull, A. R., Bacteriophages as enteric viral indicators in bivalve mollusc management. *Food Microbiol.* **2017,** *65*, 284-293.
19. Ahmed, S. R.; Takemeura, K.; Li, T.-C.; Kitamoto, N.; Tanaka, T.; Suzuki, T.; Park, E. Y., Size-controlled preparation of peroxidase-like graphene-gold nanoparticle hybrids for the visible detection of norovirus-like particles. *Biosens. Bioelectron.* **2016,** *87*, 558-565.
20. Tian, P.; Mandrell, R., Detection of norovirus capsid proteins in faecal and food samples by a real time immuno-PCR method. *J. Appl. Microbiol.* **2006,** *100*, 564-574.